Trans. JSASS Aerospace Tech. Japan
Vol. 10, No. ists28, pp. Pe_21-Pe_30, 2012

Original Paper

Thermal Response Analysis of Low-Density CFRP Ablator

By Toshiyuki SUZUKI[1)], Kazuhisa FUJITA[1)], Takeharu SAKAI[2)], Kei-ichi OKUYAMA[3)], Sumio KATO[4)] and Seiji NISHIO[5)]

[1)]*Japan Aerospace Exploration Agency, Chofu, Japan*
[2)]*Dept. of Aerospace Engineering, Nagoya University, Nagoya, Japan*
[3)]*Graduate School of Engineering, Aichi University of Technology, Gamagouri, Japan*
[4)]*Graduate School of Engineering, University of The Ryukyus, Nakagami, Japan*
[4)]*Aerospace Company, Kawasaki Heavy Industry, LTD., Kakamigahara, Japan*

(Received June 16th, 2011)

The thermal characteristics of the low-density ablator are quantified by conducting the heating tests of materials in an arcjet wind tunnel. In the tests, test pieces of the ablator with a diameter of 40mm and a length of 58mm are put into arcjet flow. The arcjet wind tunnel is run for two sets of operational condition: a low heating condition for the heat flux of 0.97MW/m2 and the impact pressure of 1.93kPa, and a high heating one for 1.97MW/m2 and 4.25kPa, respectively. The surface temperature and in-depth temperature are measured during the testing. The surface shape changes of ablator and the amount of mass loss of ablator are measured after the heating tests. The obtained experimental data are analyzed by using an integrated computational method developed earlier. Agreement between the calculations and the heating tests are excellent in the comparison of the surface shape changes of ablative test pieces. The temporal variations of surface temperature are also well reproduced by the present numerical method within the experimental error. However, the calculation underestimates the in-depth temperatures and the amount of mass loss of ablative test piece. The reason for this discrepancy may come from the lack of the thermal conductivity data especially in high temperature range above 500K. In addition, the present study suggests that the thermal conduction of the ablative test piece used in this study could be anisotropic to some extent.

Key Words: Low Density Ablator, Heating Tests, Numerical Analysis

Nomenclature

H,	:	enthalpy, J/kg
I	:	electric current, A
J_s	:	mass flux of species s, kg/(m^2-s)
M_s	:	molecular weight of species s, kg/mol
$\dot{m}$	:	mass flow rate, kg/s
p	:	pressure, Pa
q	:	heat flux, MW/m^2
$\overline{R}$	:	universal gas constant, 8.314 J/(mol-K)
r	:	recession rate, m/s
S	:	recession, m
s	:	thermocouple location, mm
T	:	temperature, K
t	:	time, s
α	:	reaction probability
κ	:	thermal conductivity, W/m-K
ρ	:	density, kg/m^3
Subscripts		
av	:	average
c	:	charred material or cold wall
cl	:	centerline
eff	:	effecitve
nit	:	nitridation reaction
oxi	:	oxidation reaction
s	:	stagnation point
v	:	virgin material

1. Introduction

As a future planetary exploration mission, Japan Aerospace Exploration Agency (JAXA) has proceeded preliminary studies on a nonstop Mars sample return system using aerocapture technology named Mars Aeroflyby Sample Collection (MASC) [1)]. In this mission, the entry capsule enters into the Martian atmosphere with a velocity of 5 km/s. Because a strong detached shock wave is formed around the entry capsule during such atmospheric entry, the entry capsule is exposed to significant aerodynamic heating. For the thermal protection system (TPS) material, a low-density carbon-phenolic ablator is considered as one of strong candidate materials due to its lightweight characteristics. According to the recent development of the low-density carbon-phenolic ablator named Phenolic Impregnated Carbon Ablator (PICA)[2)], of which density is about 0.3, and is lower by about one-fifth compared with that of carbon-phenolic ablators used in the past planetary entry mission, the low-density ablator is found to be an efficient heat-shielding material. In order to design such a low-density ablator TPS for the entry capsule used in the MASC mission, a numerical method is required to predict the thermal response of a low-density ablator accurately.

As to the numerical methods of thermal response of ablator, one-dimensional computational codes were widely used in the past analyses. Well-known examples are Charring Materials Ablation (CMA) code developed by Moyer and Rindal[3)], and Fully Implicit Ablation and Thermal Response (FIAT)

program developed by Chen and Milos[4]. Other recent works were made by Ahn et al.[5], Suzuki et al.[6], and Amar et al[7]. In these analysis methods, the thermal conduction inside the ablator is calculated one-dimensionally by giving a cold wall heat flux value as a code input. The boundary condition at the ablating surface such as a blowing correction factor and a net heat flux transferred to the surface is determined by considering a surface mass and energy balance[8]. However, the application of this simple analysis method is limited because of its one-dimensional heat conduction assumption. If the curvature of ablative TPS was large, one could not assume that the heat conduction inside the ablator would be one-dimensionally. For such a case, the thermal response of ablator should be treated two-dimensionally. In addition, one cannot easily obtain the cold wall heat flux distribution for such a complicated geometry without using the computational fluid dynamics (CFD) approach.

Under these circumstances, the analysis method of thermal response of ablator has been improved, and more detailed approach has been developed for the evaluation of ablating materials. In our previous study, several computational codes were integrated to calculate the thermal response of ablator under the arcjet flow condition[9]. In the method, the thermal response of the ablator is calculated by loosely coupling between the shock layer CFD code and the two-dimensional version of ablation code using an arcjet freestream condition. The arcjet freestream condition in the test section is evaluated by calculating the flows in the arcjet wind tunnel. Using this integrated approach, the thermal response of ablator could be determined by giving a mass flow rate of working gas and an electric current of an arc heater as a code input. Recently, the developed integrated analysis method has been applied to the heating tests conducted in the 1 MW arcjet wind tunnel at the Institute of Space and Astronautical Science (ISAS) of JAXA[9] and the 750 kW arcjet wind tunnel at Aerospace Research and Development Directorate (ARD) of JAXA[10]. In these analyses, the temporal changes of surface temperature and in-depth temperature of ablative test pieces with a specific gravity value of about 1.5 were calculated by using the integrated method. The obtained results were also compared with those obtained in the heating tests. It was found from the studies that the measured surface temperatures were reproduced well by the integrated method using the noncatalytic wall boundary condition, though the agreement between the calculation and the heating tests became slightly worse for in-depth temperature due to the lack of thermal conductivity data especially in high temperature regime. However, it is still unknown that the integrated analysis method can be applied to other ablative materials such as low- or medium-density ablators with a specific gravity value from 0.3 to 1.0. For future planetary entry missions, it is important to examine the prediction accuracy of the numerical methods mentioned for the low-density ablator.

In order to examine the prediction accuracy of the numerical methods mentioned above, several experimental data are required in this study. Two major requirements are given as follows:

(1) We need the experimental results obtained in the heating tests of low-density ablator. The heating tests are usually carried out in the arcjet wind tunnel. In the heating tests, the ablative test piece is put into a hot arcjet flow. The time variations of surface temperature and in-depth temperature of the ablative test piece are measured during the testing. The obtained data are used to validate the calculated results obtained by the numerical results.

(2) In order to calculate the thermal responses of ablator by using the numerical methods, a lot of material information about the ablator will be required. In particular, density values for virgin and char materials of ablator and the thermal properties such as thermal conductivity are necessary to analyze the experimental data obtained in the heating tests. Thermal gravimetric analysis (TGA) data is also required to characterize the pyrolysis phenomena.

The ultimate aim of the present study is to develop the numerical method that can predict the thermal response of low-density ablator under high temperature. For this purpose, we examine whether or not the integrated analysis method can predict the thermal response of low-density ablator. In the present study, the heating tests of low-density ablator are first carried out in the 750 kW arcjet wind tunnel in ARD of JAXA. In the tests, the surface temperature and temperatures inside the ablative test piece are measured during the testing. The surface recession and the shape change due to surface reactions under high temperature are evaluated after the heating tests. To develop the thermal response model of the ablator used in this study, the thermal conductivity are measured by using the steady-state method. TGA is made to model the pyrolysis phenomena of low-density ablator. Based on the measured values, the regression analyses are made to develop the numerical models for the low-density ablator. The obtained models are then introduced into the integrated analysis method. Finally, the thermal responses of ablator under the arcjet flow conditions are analyzed by using the integrated analysis method. The calculated results are compared with experimental data obtained in the heating tests.

2. Heating Tests

The heating tests of low-density ablator were carried out in the 750 kW arcjet wind tunnel in ARD of JAXA. The ablative material used in this study was developed by Aichi University of Technology, and is named Lightweight Ablator series for Transfer vehicles (LATS). The LATS is a carbon-phenolic ablator fabricated by impregnating a phenolic resin into a felt made of carbon fiber.

Figure 1 shows the schematic diagram of the ablative test piece used in the present study. The test piece has a diameter of 40mm and a length of 58 mm. The thickness of the LATS ablator is 40 mm. As shown in Fig. 1, one thermocouple (Type K) is inserted into the each ablative test piece along the centerline from the back surface. The thermocouple locations are summarized in Table 1. The surface temperature is measured by using a two-color optical pyrometer.

Test conditions and the wind tunnel operational parameters are summarized in Table 1. In this study, air is used as a working gas. The arcjet wind tunnel is run for two sets of

Table 1. Wind tunnel test conditions.

Test piece			Test conditions								
No.	ID	Density (kg/m^3)	s (mm)	Gas	$\dot{m}$ (kg/s)	I (A)	q_c (MW/m^2)	p_s (kPa)	H_{cl} (MJ/kg)	H_{av} (MJ/kg)	t (s)
1	H1B1-01	295.2	20	Air	0.01	300	0.97	1.93	19.8	11.8	60
2	H1B1-02	319.2									
3	H1B1-03	338.8									
4	H1B2-01	350.2	30								
5	H1B2-02	389.1									
6	H1B2-03	284.5									
7	H2B1-01	303.6	20	Air	0.02	700	1.97	4.25	28.7	18.0	60
8	H2B1-02	333.2									
9	H2B1-03	305.5									
10	H2B2-01	363.5	30								
11	H2B2-02	351.7									
12	H2B2-03	328.2									

operational condition: a low heating condition is chosen for mass flow rate of 0.01 kg/s and electrical current of 300 A; and a high heating one for 0.02 kg/s and 700 A, respectively. The measured heat flux and the impact pressure values are 0.97 MW/m^2 and 1.93 kPa for the low heating condition, and 1.97 MW/m^2 and 4.25 kPa for the high heating condition, respectively. The heater thermal efficiency is measured and the obtained Mass-averaged enthalpy value is 11.8 MJ/kg, and 18.0 MJ/kg for the low and high heating cases, respectively. Centerline enthalpy values are evaluated by using a computer code to calculate arcjet flows[11, 12]. The evaluated centerline enthalpy value is about 19.8 MJ/kg, and 28.7 MJ/kg, respectively. The testing time for the experiments is 60 seconds. In the heating test, the ablative test piece is put into arcjet flow at t=0s, and then it is retracted immediately after the prescribed exposure time of has elapsed.

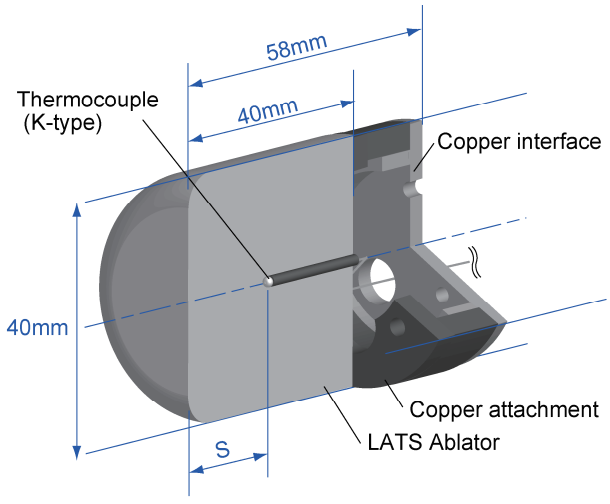

Fig. 1. Schematic of ablative test piece used in this study.

3. Integrated Thermal Response Analysis of Ablator

In the course of the simulation, the thermal response of ablator under arcjet flow condition is obtained through a coupled manner developed in our previous study[9, 10]. In the coupled method, the thermal response is analyzed by using different computational tools. Three computational blocks are built in the present study. 1) simulation of the entire flowfield in an arcjet wind tunnel facility from an upstream end of an upstream electrode chamber to a test section, 2) simulation of thermochemical nonequilibrium shock layer flowfield over an ablator test piece, and 3) simulation of thermal conduction within the ablator test piece. Though some of the details are given in our previous papers[9, 10], the brief explanation of the procedure is explained below for completeness.

3.1. Simulation of flowfiled in 750 kW arcjet wind tunnel

In order to calculate the flowfield around ablative test piece, we need to know the arcjet freestream condition. The arcjet flow is heated to a high enthalpy condition through an electric discharge and thus the flow is highly dissociated and ionized. When the arcjet flow is expanded through nozzle, density is so low that the recombination process is not completed. Therefore, the concentration of the atomic species in the arcjet freestream is greater than that calculated by the equilibrium relationship. This amount of the atomic species needs to be known for the present analysis. For this purpose, the numerical simulation of flowfield in arcjet wind tunnel is carried out in this study.

Two subblocks are further built to calculate the flowfield in the 750 kW arcjet wind: one subblock represents the arc heater section from the upstream electrode chamber to the nozzle throat and another represents the nozzle section downstream of the nozzle throat. In the arc heater section, the flow is solved using the ARC heater FLOwfield 3 (ARCFLO3) code[11]. Solutions are obtained by numerically integrating the Navier-Stokes equations in time to steady state by using mass flow rate and electrical current as the code input. The nozzle section is simulated by a thermochemical nonequilibrium CFD code[12]. Note that inlet boundary condition is given by the ARCFLO3 solutions at the throat. Because the numerical methods used in these two codes can be found in Refs. 11 and 12, the details are omitted here. Figure 2 shows the computational grid for the 750 kW arcjet wind tunnel. The number of 180×40 cells is used for the arc heater region, and that of 250×50 cells for the nozzle region. As is shown in Fig. 2, an equivalent nozzle extends past the

physical exit location to calculate the flow properties at the axial location of the testing of the ablator. The half-angle of the equivalent nozzle is determined to duplicate the measured pitot pressure value[12]. The flow properties at the axial location of the testing were discussed in Ref. 10).

3.2. Simulation of flowfield around ablative test piece

The thermochemical nonequilibrium CFD code is used for the computation of an ablating shock layer flowfield. The governing equations are the Navier-Stokes equations for axisymmetric flowfield, consisting of species mass, momentum, total energy, and vibronic energy conservation equations. For high temperature airflow, we employ the following 11 chemical species: N, O, N_2, O_2, NO, N^+, O^+, N_2^+, O_2^+, NO^+, and e-. Moreover, we consider the following 10 species as the ablation product gas: C, C_2, CN, CO, C_3, C^+, H, H_2, H^+, and C_2H. Park's two-temperatire model is employed to determine the thermochemical nonequilibrium states.

In the present study, we consider the following three types of chemical reactions that occur at the ablator surface: 1) oxidation by atomic oxygen that produces CO, 2) nitridation by atomic nitrogen that produces CN, and 3) sublimation that produces C_3. Mass fluxes of CO and CN due to oxidation and nitridation reactions are given by

$$J_{CO} = \frac{M_{CO}}{M_O}\rho_O \frac{\alpha_{oxi}}{4}\sqrt{\frac{8\bar{R}T}{\pi M_O}}, \tag{1}$$

$$J_{CN} = \frac{M_{CN}}{M_N}\rho_N \frac{\alpha_{nit}}{4}\sqrt{\frac{8\bar{R}T}{\pi M_N}}. \tag{2}$$

The reaction probability of oxidation reaction is taken from Ref. 13). As for the probability of nitridation reaction, the numerical model has been proposed in Ref. 14). The mass flux of C_3 due to sublimation reaction, J_{C_3}, is given by Hertz-Knudsen-Langmuir equation[15]. The surface of ablative material is assumed to be noncatalytic to atomic oxygen and atomic nitrogen for all the computed cases in the present study, because it is found from in a past experimental study that the catalytic recombination reaction by those atomic specied hardly occurs at carbon surface[16-18].

It should be noted that the flowfield over the ablating surface is calculated by accounting for the modified shape of test piece via the coupled calculation. The recession rate at each grid point is obtained from the CFD solutions as

$$r = \frac{M_C}{M_{CO}}\frac{J_{CO}}{\rho_c} + \frac{M_C}{M_{CN}}\frac{J_{CN}}{\rho_c} + \frac{M_C}{M_{C_3}}\frac{J_{C_3}}{\rho_c}. \tag{3}$$

The amount of surface recession at a certain time point is obtained by integrating the recession rate and is given by

$$S = \int_0^{t_i} r dt. \tag{4}$$

In the course of the present analysis, the mass fluxes of CO, CN and C_3 are obtained from the converged solution of the flowfield analysis around the ablative test piece. With the mass flux values so obtained, the amount of surface recession in the normal direction to the surface is calculated by using Eqs. (3) and (4).

3.3. Thermal response analysis of ablator

The thermal response of ablative test piece is calculated by the SCMA2 code[9]. In the SCMA2 code, two conservation equations, that is, conservation of solid density and energy equations are solved two-dimensionally.

$$\frac{\partial \rho}{\partial t} = -R, \tag{5}$$

$$\rho c_p \frac{\partial T}{\partial t} = \nabla\cdot(\kappa\nabla T) - (h_g - \bar{h})\nabla\cdot\dot{m}_g + \dot{m}_g \nabla h_g. \tag{6}$$

The energy conservation equation is a transient heat conduction equation with additional term. The individual terms is interpreted as follows: rate of storage of energy, net rate of thermal conductive heat flux, heat-absorbing due to the thermal decomposition, and the energy transport by the pyrolysis gas motion. In order to solve the equation numerically, thermal conductivity data of ablative material is required. Because the thermal conductivity is presently unknown, the thermal conductivity will be measured in this study. The detail of the procedure will be shown later.

The solid density conservation equation has a pyrolysis term to account for the density change of ablator due to the

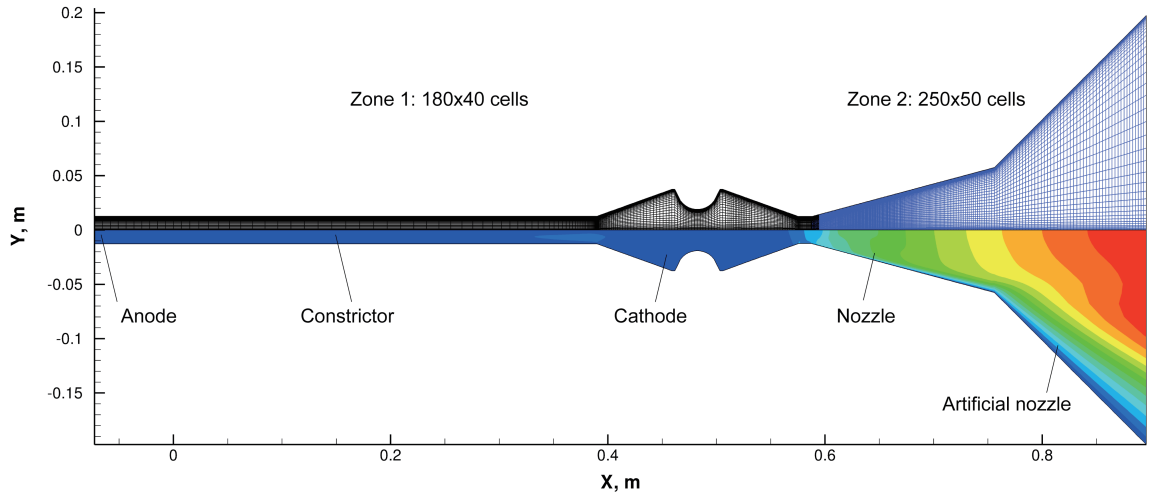

Fig. 2. Computational mesh for 750 kW arcjet wind tunnel in ARD of JAXA (top) and typical example of converged solution for the case of the low heating condition (I = 300 A, $\dot{m}$ = 0.01 kg/s). Mach number contours in zones 1 and 2 are shown (bottom).

thermal decomposition. The pyrolysis term is expressed as follows:

$$R = \sum_{k=1}^{N} f_k A_k \exp\left(-\frac{B_k}{T}\right)(\rho_v - \rho_c)\left(\frac{\rho_s - \rho_c}{\rho_v - \rho_c}\right)^{\mu_k} . \quad (7)$$

In the present study, all parameters used in Eq. (7) are determined to reproduce the thermograms of the TGA data. The detail of the procedure will be shown later.

The motion of pyrolysis gas is assumed to be one-dimensional along the direction perpendicular to the ablator surface η, and the mass flux of pyrolysis gas is calculated using following approximation,

$$\dot{m}_g = \int R d\eta . \quad (8)$$

The chemical composition of the pyrolysis gas at the wall surface is calculated by assuming thermochemical equilibrium condition.

The thermal response analysis needs two boundary conditions: heat flux and recession rate. The heat fluxes and recession rate at each position along the ablator surface must be known as a function of time. An iterative procedure is used to obtain the consistency of the two boundary conditions between the thermal response analysis and the flowfield calculation over the test piece, which will be explained in the next subsection. Based on our experience in our previous work[9], three iterations are needed to obtain convergence at a given time. This procedure must be repeated to obtain a time-dependent solution for total testing time.

Because this procedure is very time-consuming, several time points need to be chosen practically. Ideally, the interval between two time points should be short because the phenomenon over the ablative test piece is unsteady. When we made a coupling calculation by setting a time interval equally to be 5s until the end of testing, the calculated surface contour of the test piece was totally different from the heated test piece. This qualitatively different contour was likely due to insufficient time resolution during the first 5s from the beginning of testing: In that case, the temperature and atomic species density distributions over the surface of the test piece changed dramatically in the first 5s, but remained keeping unphysical after t=10s. As a result, we added two time points prior to t=5s and fourteen points at t= 1, 3, 5, 10, 15, 20, 25, 30, 35, 40, 45, 50, 55 and 60s were selected for the present study. The computing time of the coupled calculation is about 340h (two weeks) by using two dual core processors (Intel® Xeon® 5050) installed in a Dell Precision workstation 690.

A typical example of computational meshes for both flowfield and ablative test piece are shown in Fig. 3. The zone 3 with 77×50 cells is used for the flowfield calculation. Note that the computational domain for the ablator is divided into two subzones. The zone 4a has 77×50, and the zone 4b has 29×48 cells. The zone 3 and zone 4a are required to account for the surface shape change of ablator due to surface reactions occurred at the ablating surface. When the shape of the ablative test piece changes, the outer boundary in zone 4a (corresponds to the surface of the ablative test piece) is redefined accordingly and new numerical mesh system is redrawn to construct zones 3 and 4a. The grid points in zone 4b remain fixed in the course of simulation.

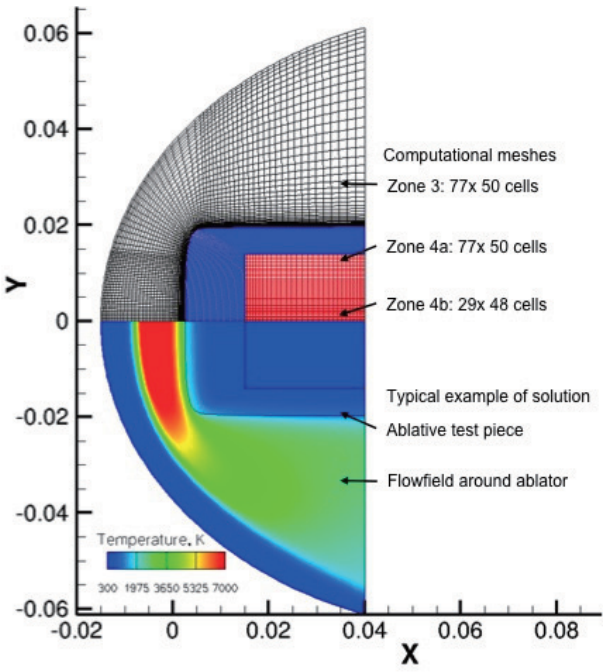

Fig. 3. Computational meshes for flowfield calculation and thermal response analysis of ablator (top), and typical example of solution for the case of the low heating condition ($I = 300$ A, $\dot{m} = 0.01$ kg/s). Temperature contours at $t = 60$s from the onset of heating are shown (bottom).

4. Thermal Properties & Numerical Models of LATS

The density values of virgin LATS ablator are measured by weighing the test piece materials. The obtained values are listed in Table 1. The arithmetic mean and the standard deviation of virgin density are 330.23 kg/m^3 and 30.6 kg/m^3, respectively. This density value will be used in the thermal response analysis, and is also listed in Table 2.

To characterize the mass loss due to the pyrolysis phenomena of the present LATS ablator, the TGA was carried out by using the TG/DTA6300 system (Seiko Instruments Inc.). The obtained data is shown in Fig. 4. For the purpose of comparison, the results are presented for the virgin density of about 300, 500, 700 kg/m^3. The TGA was performed in an argon atmosphere with prescribed heating rates of 10 K/min. The weights of ablative test piece used in this measurement are about 15mg. As shown in Fig. 4, the LATS ablator begins to pyrolyze from 500 K, and is strongly pyrolyzed from 600 K. The weight loss curve becomes nearly constant over 1000 K for the virgin density of 300 kg/m^3. The resulting weight loss is about 70 % of the original mass of the test piece. Almost the same situation can be seen for the cases of 500 and 700 kg/m^3. Base on this result, the density value for charred material is estimated to be 231.16 kg/m^3 ($\rho_v \times 0.70$). This density value will be used in the thermal response analysis, and is also listed in Table 2.

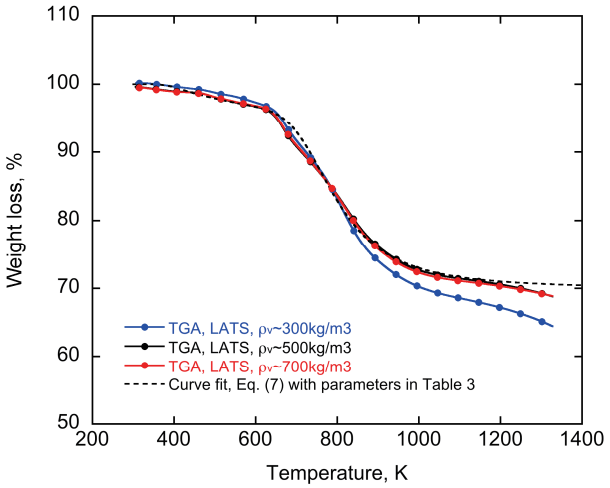

Fig. 4. Thermal gravimetric weight loss histories for several LATS ablative test piece.

Table 2. Calculation condition.

Density of virgin material, ρ_v	330.23 kg/m^3
Density of charred material, ρ_c	231.16 kg/m^3
Emissivity, ε	0.85

Table 3. Curve fit parameters in Eq. (7) for pyrolysis model.

Parameters	$k=1$	$k=2$
A_k	0.10	0.90
B_k	3.50E9	7.00E9
f_k	1.10E4	1.10E4
μ_k	100.0	3.0

Based on the obtained TGA data, a regression analysis is made by using Eq. (7). In this analysis, Eq. (5) is integrated numerically with time by varying the parameters in Eq. (7): A_k, B_k, f_k and μ_k. These parameters are determined by trial and error method to reproduce the weight loss data in Fig. 4. It is found that two components expression, $N=2$, is enough to give a satisfactory curve. The results are also presented in Fig. 4, and the curve-fit parameters used in Eq. (7) can be found in Table 3.

In order to analyze the thermal response of ablator, the thermal conductivity values of the virgin materials are measured by using a steady-state method (ULVAC-RIKO, GH-1). The obtained values are summarized in Fig. 5. The results are presented for the virgin density of about 300, 500, 600, and 900 kg/m^3. For the purpose of comparison, the thermal conductivity values of a generic CFRP ablator[10] which has a virgin density of about 1500 kg/m^3 and the values of Phenolic Impregnated Carbon Ablators (PICA)[19] which has a virgin density of about 300 kg/m^3 are also shown in Fig. 5. From Fig. 5, one can see that the thermal conductivity values of LATS ablator become smaller than those of the generic ablator. In addition, the thermal conductivity value decreases as the density value becomes small. This trend is because the smaller the density of ablator becomes, the more porous the ablative materials become. It should be noted that the thermal conductivity values obtained for LATS ablator are quantitatively similar with those of PICA. This trend is because the density values of LATS ablator become almost the same as those of PICA.

Based on the obtained thermal conductivity data, a regression analysis is made by using a following linear function of temperature:

$$\kappa = AT + B\,. \tag{9}$$

The curve fit parameters used in Eq. (9) are summarized in Table 4. In the present analysis, the curve fit parameters obtained for 300kg/m^3 are used because the arithmetic mean of virgin density used in the heating tests is 330kg/m^3.

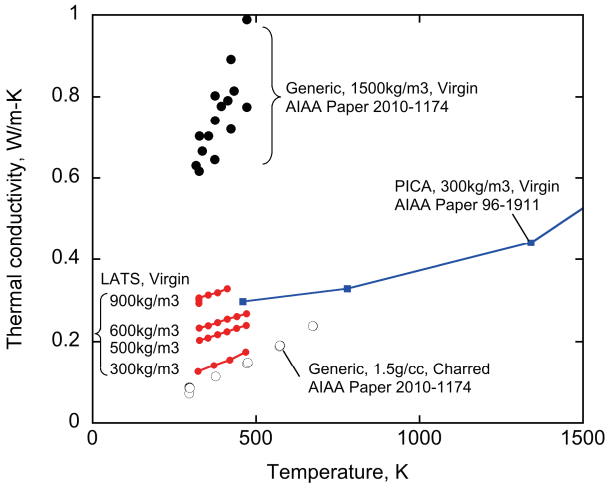

Fig. 5. Thermal conductivity values obtained for the present LATS ablator.

Table 4. Curve fit parameters in Eq. 9 for thermal conductivity models.

Density of LATS Ablator	A	B
300 kg/m^3	3.2778E-4	2.0323E-2
500 kg/m^3	3.4042E-4	7.3316E-2
600 kg/m^3	2.5743E-4	1.1915E-1
900 kg/m^3	3.2316E-4	1.9597E-1

5. Results & Discussions

The heating tests using the LATS ablator test piece are conducted in the 750 kW arcjet wind tunnel for the wind tunnel operational parameters shown in Table 1. Typical example of the operation is shown in Fig. 6.

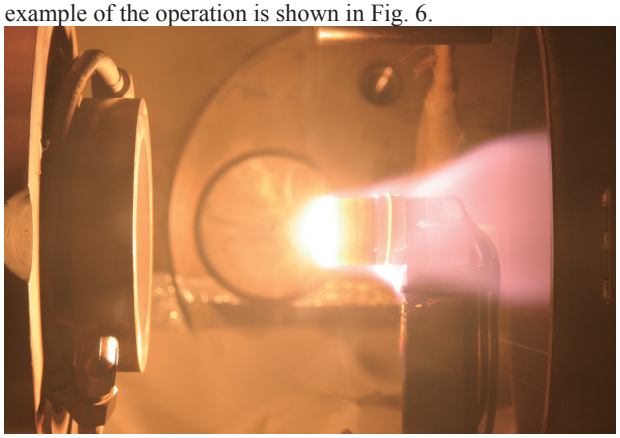

Fig. 6. Low-density ablator test piece (H2B1-01) put into arcjet flow. ($\dot{m}$=0.02 kg/s, I=700 A)

According to Lundell et al.[20], the efficiency of the ablative

material can be quantified by using an effective heat of ablation, which is expressed as follows:

$$H_{eff} = \frac{q_c}{r\rho_v}. \tag{10}$$

where q_c is the cold wall heat flux at the stagnation point, r is recession rate (average recession divided by test time), and ρ_v is the density of virgin material. The obtained results are shown in Fig. 7. For the purpose of comparison, the values obtained for PICA ablator[19] are also shown in the same figure. As shown in Fig. 7, the material efficiency of the LATS ablator becomes comparable with that of PICA ablator, although our testing condition is limited in lower cold wall heat flux compared with the testing condition for PICA.

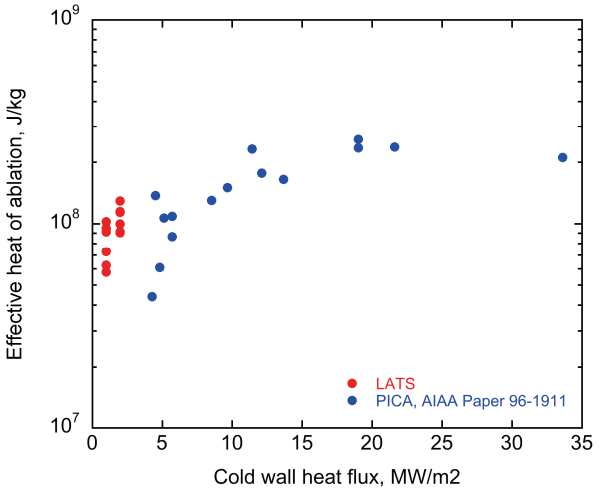

Fig. 7. Comparison of effective heat of ablation between LATS and PICA ablator.

Figure 8 shows the surface temperature variations at the stagnation point for low and high heating conditions, respectively. The results are presented for the calculations using the present integrated method and the measurements. From Fig. 8, one can see that the measured temperature increases rapidly from the onset of heating. After that, the surface temperature becomes almost constant at 2,000 K for low heating condition, while the temperature reaches up to 2,500 K for high heating condition. Repeatability is fairly good except for the beginning of exposure.

From Fig. 8, one can see that the calculated temperature duplicates well the measured values for low heating condition, though the calculation slightly underestimates the measured one for high heating condition. Because the experimental uncertainty is estimated to be ±5 % in the surface temperature, it is considered that the agreement between the calculations and the measurements is fairly good for both heating conditions.

The in-depth temperatures are shown in Fig. 9 for low heating condition. The results are shown in Fig. 9(a) for the measurement, and are shown in Fig. 9(b) for the calculation. From Fig. 9(a), the temperature measured at 20mm from the surface increases from the onset of heating, and becomes the maximum of 650 K at 120s. After that, the temperature decreases gradually due to the radiative cooling effect from the ablating surface. The temperature measured at 30 mm from the surface becomes lower by 100 K than that measured at 20 mm. By comparing the temperature variations measured at 20 mm and 30 mm, it is found that the repeatability of temperature measurements becomes worse for the case of 20 mm. This trend is because it is difficult to set a thermocouple junction accurately at the bottom of a pinhole of ablator test piece. Even a small gap between the ablative test piece and the thermocouple junction affects the variation of in-depth temperature.

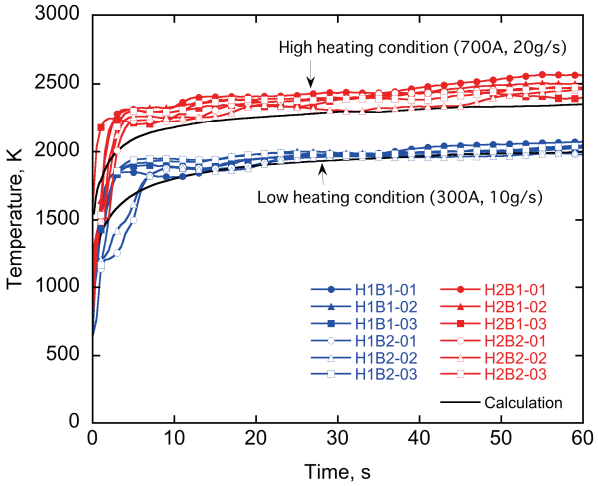

Fig. 8. Temporal variations of surface temperature at the stagnation point both for low and high heating conditions.

By comparing Figs. 9(a) and 9(b), one can see that the calculated results (denoted as isotropic) underestimate the measurements both for 20 mm and 30 mm from the surface. In addition, the calculated temperature at 30 mm from the surface increases more slowly than that at 20 mm, unlike the measured results shown in Fig. 9(b). The reasons for these differences are currently unknown. One possible reason is that the present LATS ablator could have an anisotropic nature in thermal conduction. In the present study, the thermal conductivity values of LATS ablator in the direction parallel to the arcjet flow are measured, and the thermal conduction is assumed to be isotropic. If the LATS ablator had an anisotropic nature in thermal conduction, and if the thermal conductivity in the direction perpendicular to the arcjet flow became larger than that in the direction parallel to the arcjet flow, the in-depth temperature could become larger than that obtained by assuming isotropic thermal conduction due to the heat input from the sidewall of the test piece.

The calculated results obtained by assuming such anisotropy in thermal conduction are also shown in Fig. 9(b). As shown in this figure, the maximum temperature increases with the degree of anisotropy in the thermal conduction, and the qualitative trends in the in-depth temperature become close to the measurements. However, the quantitative trends that the temperature measured at 30 mm from the surface became lower by 100 K than that measured at 20 mm could not reproduced even when the anisotropic nature of the LATS ablator is assumed in the present calculations. The reason for this discrepancy may come from the lack of the thermal

conductivity data especially in high temperature range above 500 K. This point needs to be improved in the future. Because the almost the same situation can be seen for high heating conditions, the results are omitted here.

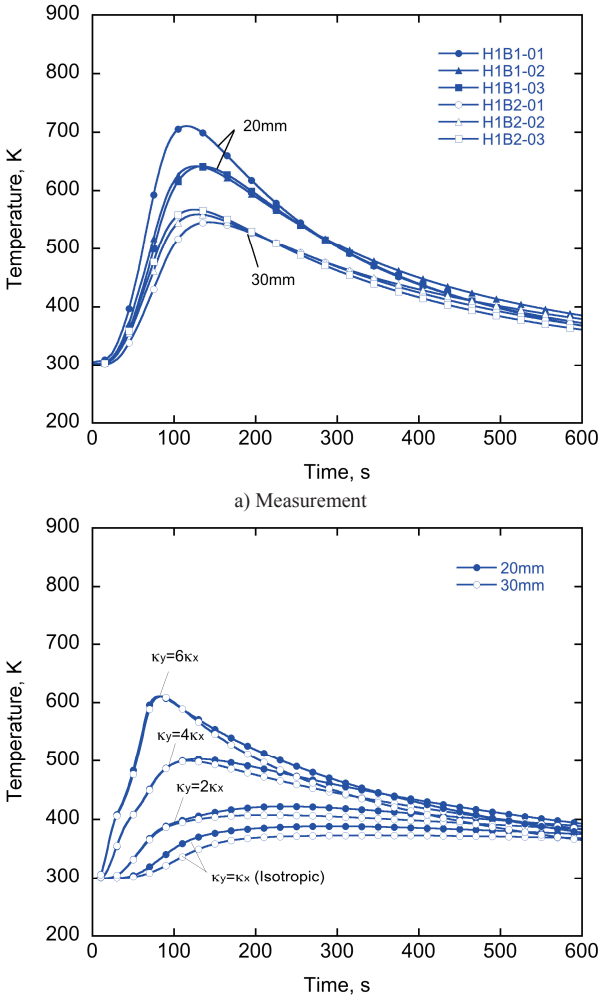

Fig. 9. Time variations of in-depth temperature along the centerline of ablative test piece for low heating condition.

After the heating tests, ablative test pieces were put on graph paper with a scale, and we took a photograph of each of them. The original coordinate data of the ablator surface were digitized by scanning the photograph. The experimental uncertainty of the coordinate so digitized is estimated to be less than ±0.5 mm. The obtained results are shown in Fig. 10(a) for low heating condition, and are shown in Fig 10(b) for high heating case. From Figs. 10(a) and 10(b), one can see that the amount of surface shape change for high heating condition becomes larger than that for low heating one. This trend is because the surface temperature for high heating condition becomes larger than that for low heating case, as was shown in Fig. 8. In addition, the degree of dissociation of molecular oxygen and nitrogen for high heating condition would become larger than that for low heating case due to higher power input. As a result, the surface reactions that produce CO and CN occurred significantly for high heating condition, as was given in Eqs. (1)~(3).

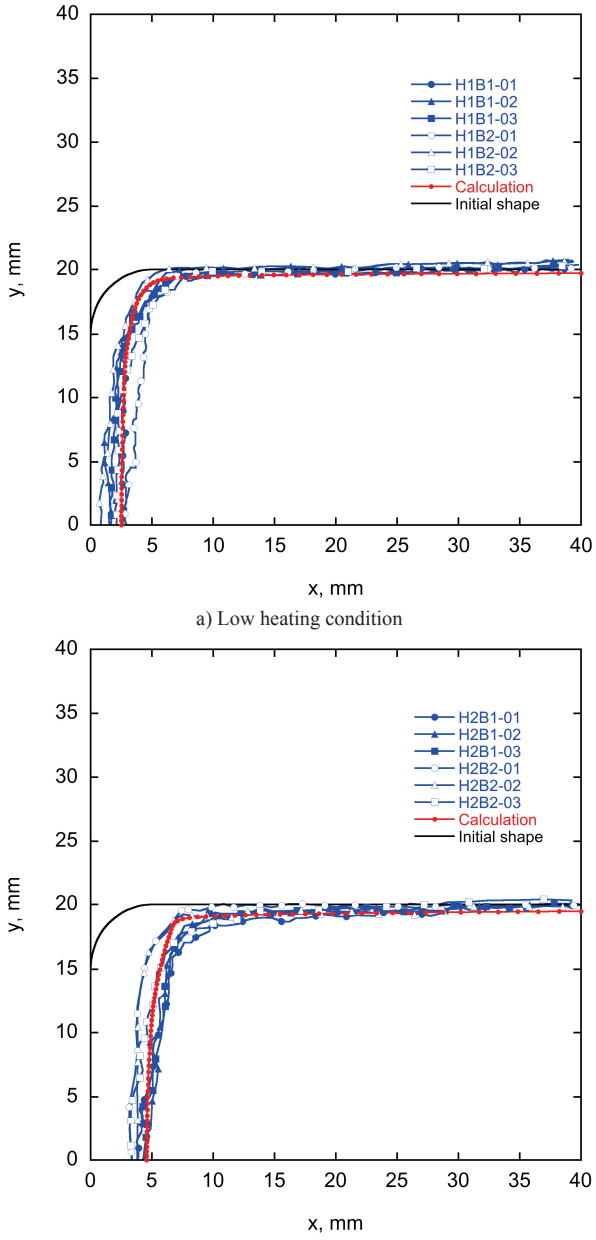

Fig. 10. Comparison of surface shape of ablative test piece after the heating test between the calculation and the measurement.

As shown in these figures, the experimental results are characterized by very strong scattering along the test piece surface. This trend is believed to occur due to an individual difference of test pieces. As was mentioned in the beginning of Section 4, the arithmetic mean and the standard deviation of density values of ablative test piece are 330.23 kg/m^3 and 30.6 kg/m^3, respectively. This implies that density values and a degree of impregnation of resin into carbon felt would be slightly different from each other even if some of these test pieces came from the same block, piece or lot. As a result, the amount of surface shape change was different from each other. At the stagnation point, the arithmetic mean and the standard

deviation of surface recessed distance are 1.951 mm and 0.683 mm for the low heating condition, and 3.861 mm and 0.415 mm for the high heating one, respectively.

In Figs. 10(a) and 10(b), the calculated results are also presented. From figures, one can see that the agreements between the calculation and the measurement are excellent both for the low and high heating conditions. This good agreement was achieved because the present numerical method could predict the surface temperature and the amount of atomic species striking onto the ablative surface reasonably. As a result, the calculated surface shape changes due to the oxidation and nitridation reactions agree well with those of measured, as was given in Eqs. (1)~(3).

After the heating tests, the ablative test pieces were weighed to obtain the amount of mass loss of the ablative test piece. The obtained results are shown in Fig. 11. The results are presented for the measurement and the calculation. For the calculation, the results are shown for the cases of isotropic and anisotropic thermal conduction of ablative test piece. When the ablator is heated, the ablator loses its weight due to the thermal decomposition of phenolic resin as well as the surface reactions. Those distinctions are also given in the figure. In our testing condition, the amount of mass loss is typically 4.32 g for low heating condition, and 6.00 g for high heating case, respectively. The amount of mass loss for high heating condition becomes about 1.4 times larger than that for low heating one. This trend is because the surface temperature for high heating condition becomes higher than that for low heating case, as was shown in Fig. 8. As a result, the amount of mass loss of ablative test piece due to the surface recession and the amount of thermal decomposition of resin increases for the high heating condition.

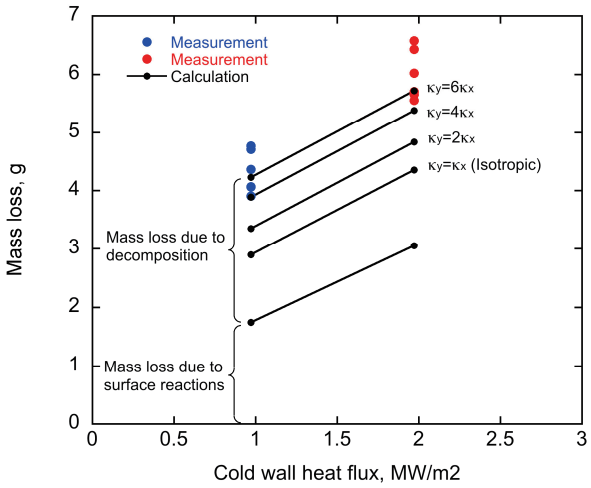

Fig. 11. Comparison of mass loss of ablative test piece between the low and high heating conditions.

As shown in Fig. 11, the calculated results obtained by assuming the isotropic thermal conduction underestimate the measurements both for low and high heating conditions. However, this disagreement could be improved by assuming the anisotropic nature in thermal conduction. From Fig. 11, one can see that the amount of mass loss of ablative test piece increases with the degree of anisotropy in the thermal conduction. In addition, the quantitative trends become close to the measurement for the case of $\kappa_y = 6\kappa_x$. This trend is believed to occur because the in-depth temperature for the anisotropic case becomes larger than that for the isotropic case due to the heat input from the sidewall of the test piece, as was shown in Fig. 9(b). As a result, the thermal decomposition inside the ablative test piece proceeds significantly for the anisotropic case resulting in larger mass loss of ablative test piece.

6. Summary

Heating tests of the LATS ablator were carried out in 750kW arcjet wind tunnel facility in ARD of JAXA. Surface temperature and temperature inside ablative test piece were measured during the testing. The amount of mass loss and surface shape changes were evaluated after the heating test. The measurements of the thermal conductivity values and the thermogravimetric analysis were made by using the LATS test pieces. Based on the measured data, thermal response models for the LATS ablator were developed, and they were introduced into the integrated analysis method. The thermal responses of ablator under the arcjet flow conditions so obtained were analyzed by using the integrated analysis method. The calculated results were compared with experimental data obtained in the arcjet wind tunnel.

Excellent agreement between the calculations and the heating tests are obtained in the surface shape changes after the heating tests. The temporal variations of surface temperature are also well reproduced by the present numerical method within the experimental error. On the other hand, the agreement between the calculation and the measurement becomes poor in the comparison of the in-depth temperature and the amount of mass loss of ablative test piece. The reason for this discrepancy may come from the lack of the thermal conductivity data especially in high temperature range above 500 K. In addition, the present study suggests that the LATS ablator has an anisotropic nature in the thermal conduction to some extent.

Acknowledgments

Authors would like to thank here all the student that joined the 2010 summer internship program in JAXA and supported our the heating test program: Teruhiko Kanada, Hiroaki Tsuzuki from Aichi University of Technology, Takahiro Inoue, Mitsunobu Kuribayashi, Takuya Mori from Nagoya University, Kenta Gibo from University of The Ryukyus, and Jun Shimokawadoko from Kyushu University.

References

1) Fujita, K., Tachibana, S., Sugita, S., Miyamoto, H., Mikouchi, T., Suzuki, T., Takayanagi, H., Ozawa, T., Kawaguchi, J. and Woo, H.: Nonstop Mars Sample Return System Using Aerocapture Technologies, AIAA Paper 2009-5614, AIAA Atmospheric Flight Mechanics Conference, 10-13 August 2009, Hyatt Regency McCormick Place, Chicago, Illinois.

2) Tran, H. K., NASA, Johnson, C. E., Rasky, D. J., Hui, F., Hsu, M.-T., Chem, H.C. and Chen, Y. K.: Phenolic Impregnated

Carbon Ablators (PICA) for Discovery Class Missions, AIAA-1996-1911, Thermophysics Conference, 31st, New Orleans, LA, June 17-20, 1996.
3) Moyer, C. B. and Rindal, R. A.: An Analysis of the Coupled Chemically Reacting Boundary Layer and Charring Ablator, Part II: Finite Different Solution for the In-Depth Response of Charring Materials Considering Surface Chemical and Energy Balances, NASA CR-1061, June 1968.
4) Chen, Y.-K. and Milos, F. S.: Ablation and Thermal Response Program for Spacecraft Heatshield Analysis, *Journal of Spacecraft and Rockets*, **36** (1999), pp. 475-483.
5) Ahn, H.-K., Park, C. and Sawada, K.: Response of Heatshiled Material at Stagnation Point of Pioneer-Venus Probes, *Journal of Thermophysics and Heat Transfer*, **16** (2002), pp. 432-439.
6) Suzuki, T., Sawada, K., Yamada, T. and Inatani, Y.: Experimental and Numerical Study of Pyrolysis Gas Pressure in Ablating Test Piece, *Journal of Thermophysics and Heat Transfer*, **19** (2005), pp. 266-272.
7) Amar, A., Blackwell, B. and Edwards, J.: Development and Verification of a One-Dimensional Ablation Code Including Pyrolysis Gas Flow, *Journal of Thermophysics and Heat Transfer*, **23** (2009), pp. 59-71.
8) Potts, R. L.: Hybrid Integral/Quasi-Steady Solution of Charring Ablation, AIAA Paper 90-1677. June 1990.
9) Suzuki, T., Sakai, T. and Yamada, T.: Calculation of Thermal Response of Ablator Under Arcjet Flow Condition," *Journal of Thermophysics and Heat Transfer*, **21** (2007), pp. 257-266.
10) Suzuki, T., Fujita, K., Sakai, T., Okuyama, K., Kato, S. and Nishio, S.: Evaluation of Prediction Accuracy of Thermal Response of Ablator Under Arcjet Flow Conditions, AIAA Paper 2010-4787, 10th AIAA/ASME Joint Thermophysics and Heat Transfer Conference, 28 June-1 July 2010, Hyatt Regency McCormick Place, Chicago, Illinois.
11) Sakai, T.: Computational Simulation of High-Enthalpy Arc Heater Flows, *Journal of Thermophysics and Heat Transfer*, **21** (2007), pp.77-85.
12) Sakai, T., Suzuki, T, Fujita K.. and Ito, T.: Calculation of High-Enthalpy Aerothermal Environment in an Arcjet Facility, *Journal of Thermophysics and Heat Transfer*, **21** (2007), pp.249-251.
13) Park., C.: "Effect of Atomic Oxygen in Graphite Ablation," *AIAA J.*, **14** (1976), pp. 1640-1642.
14) Suzuki, T., Fujita, K. and Sakai, T.: Graphite Nitridation in Lower Surface Temperature Regime, *Journal of Thermophysics and Heat Transfer*, **24** (2010), pp. 212-215.
15) Blottner, F. G.: Prediction of Electron Density in the Boundary Layer on Entry Vehicles with Ablation, NASA SP-252, 1970, pp. 219-240.
16) Allendorf, H. D. and Rosner, D. E.: Primary Products in the Attack of Graphite by Atomic Oxygen and Diatomic Oxygen about 1100K, *Carbon*, **7** (1969), pp. 515-518.
17) Rosner, D. E. and Allendorf, H. D.: High Temperature Oxidation of Carbon by Atomic Oxygen, *Carbon*, **3** (1965), pp. 153-156.
18) Blackwood, J. D. and McTaggart, F. K.: Oxidation of Carbon with Atomic Oxygen, *Journal of Chemistry*, **12** (1959), pp. 114-121.
19) Tran, H., Johnson, C., Rasky, D., Hui, F., Chen, Y.-K. and Hsu, M.: Phenolic Impregnated Carbon Ablators (PICA) for Discovery Class Missions, AIAA Paper 96-1911, June 1996.
20) Lundell, J. H. and Dickey, R. R.: Performance of Charring Ablative Materials in Diffusion-Controlled Surface Combustion Regime, *AIAA J.*, **6** (1968), pp. 1118-1126.